Aging impairs the clustering and reduces the activity of L-type calcium channels in cardiac pacemaker cells

Matthias Baudot[1†], Oscar Vivas[1†], Sabrina Choi[1], Gabriella Serrano[1], Victor A. Flores[2], L. Fernando Santana[3], Claudia M Moreno[1*]

***For correspondence:** morenocm@uw.edu (Claudia M Moreno)

[†]These authors share co-first authorship

Present address: Department of Physiology and Biophysics. University of Washington School of Medicine. Box 357290. Seattle, WA 98195-7290. USA.

[1]Department of Physiology and Biophysics, University of Washington, Seattle, WA 98195, USA.; [2]Department of Pharmacology, University of California, Davis, CA 95616, USA.; [3]Department of Physiology and Membrane Biology, University of California, Davis, CA 95616, USA.

Abstract Every heartbeat is initiated by a spontaneous electrical signal generated inside the cardiac pacemaker. The generation of this electrical signal depends on the coordinated opening and closing of different ion channels, where voltage-gated L-type calcium channels play a central role. Despite the reliability of the pacemaker, all mammals experience a linear slowdown of the pacemaker rate with age. In humans, this slowing can become pathological and constitutes the main cause for the requirement of the implantation of artificial pacemakers. However, the mechanisms behind the age-associated slowdown of the pacemaker are not well understood. Here, we show that age directly alters the function of L-type calcium channels in pacemaker cells from mice. These age-associated alterations include: i) a reduction in the density of the channels at the plasma membrane, ii) a reduction in the clustering of the channels, iii) a decrease in channel open probability, and iv) a reduction in the cooperative gating of the calcium channels. Altogether, these age-associated alterations result in a global reduction of the L-type calcium current density and in a slowdown of the pacemaker diastolic depolarization. Remarkably, increasing the open probability of L-type calcium channels pharmacologically was enough to restore pacemaker rate in old cells to the same levels observed in the young. Overall, our findings provide evidence that proper organization and function of L-type calcium channels is impaired by aging and that this dysfunction contributes to the slowdown of pacemaker cells in old animals.

Introduction

Mammals, including humans and mice, experience a linear decline in heart rate with age ***Larson et al.*** (***2013***); ***Marcus et al.*** (***1990***); ***Ostchega et al.*** (***2011***); ***Robinson et al.*** (***1975***); ***Tanaka et al.*** (***2001***). Heart rate is dictated by the spontaneous activity of the cardiac pacemaker, a specialized tissue with the ability to fire action potentials in a spontaneous and rhythmic manner. The electrical signal originating inside the pacemaker propagates in the form of a calcium wave through the electrical conduction system of the heart, triggering the depolarization and contraction of the atrial and ventricular chambers. This cycle is repeated without interruption from embryonic development until death. The intrinsic pacemaker rate declines linearly from birth at a rate of 0.8 bpm/year in

humans and 4 bpm/month in mice ***Larson et al.*** (***2013***). This natural slowdown of the pacemaker can become pathological. In fact, the age-associated slowdown of the pacemaker is the main cause for the more than half a million artificial pacemaker devices implanted annually in the world ***Jensen et al.*** (***2014***) ***Birnie et al.*** (***2006***). However, the molecular mechanisms behind the slowdown of the pacemaker are still poorly understood.

The automaticity of the pacemaker relies on a fine balance of ionic currents that drive and allow the regeneration of the pacemaker action potential, where voltage-gated L-type calcium channels play a key role. The pacemaking mechanism can be seen as an oscillatory cycle of the membrane potential. Although oscillatory in nature, the cycle could be described starting in the diastolic depolarization (DD) phase, which can be divided in Early and Late DD. The Early DD involves the activation of hyperpolarization-activated, cyclic nucleotide–sensitive (HCN) channels ***Baruscotti et al.*** (***2005***); ***DiFrancesco*** (***1995***) and T-type $Ca_V3.1$ calcium channels ***Mesirca et al.*** (***2015***) at voltages below -60 mV. The subsequent Late DD starts at around -55 mV with the opening of L-type $Ca_V1.3$ channels ***Mesirca et al.*** (***2015***). This inward current depolarizes the membrane further enough to activate $Ca_V1.2$ L-type calcium channels at around -40 mV, pushing the membrane potential to the required threshold to trigger the action potential ***Mangoni and Nargeot*** (***2008***); ***Mesirca et al.*** (***2015***). The pacemaker action potential is a calcium action potential completely carried by the $Ca_V1.2$ and $Ca_V1.3$ L-type calcium channels. The cycle is completed by the inactivation of calcium channels and the activation of several potassium channels, including I_{to}, I_{Kur}, I_{Kr}, and I_{Ks}, resulting in the repolarization phase of the action potential ***Aziz et al.*** (***2018***). Repolarization leads to the activation of HCN channels, to start the cycle again. L-type calcium channels not only play an essential role in the generation of each action potential but also in the control of firing rate. Knockout mice lacking the $Ca_V1.3$ channel exhibit bradycardia and sinus pauses ***Baudot et al.*** (***2020***); ***Mangoni et al.*** (***2003***). In addition, humans carrying point mutations that reduce the function of $Ca_V1.3$ channels also exhibit bradycardia ***Baig et al.*** (***2011***); ***Milanesi et al.*** (***2015***), resembling the pacemaker dysfunction observed in the elderly. These observations show that $Ca_V1.3$ channels are critical for the control of action potential frequency and, consequently, heart rate.

A direct study of how aging affects the function of L-type calcium channels in cardiac pacemaker cells has been overdue for a long time. Given the key role that L-type calcium channels play in pacemaker automaticity, we hypothesized that the function of $Ca_V1.2$ and $Ca_V1.3$ channels is impaired in old pacemaker cells and that this impairment contributes to the slowdown of pacemaker rate. Combining electrophysiology, super-resolution imaging, and pharmacology, we tested this hypothesis. In this study, we determined that aging alters the organization and reduces the single channel activity and cooperativity of L-type calcium channels. As a result, pacemaker cells from old animals exhibited a reduction of their global calcium currents and a slowdown of the action potential diastolic depolarization and repolarization phases. Strikingly, increasing the open probability of L-type calcium channels in old cells was enough to restore firing rates to those values observed in the young. Our results provide evidence that alterations in L-type calcium channel function contribute to the age-associated slowdown of the pacemaker.

Results

Aging slows down the firing rate and the diastolic depolarization of pacemaker cells

Using voltage-clamp in the current-clamp configuration, we recorded the spontaneous electrical activity of isolated sinoatrial pacemaker cells from C57BL/6J mice from two age groups: 4-6 months mature adults (equivalent to 23-30 years in humans ***Flurkey et al.*** (***2007***)), and 28-30 months (equivalent to 76-81 years in humans). Figure 1B illustrates the parameters measured from the action potential waveforms to perform comparisons between young and old cells. From all the analyzed parameters, significant reductions in the old group were found for the action potential firing rate,

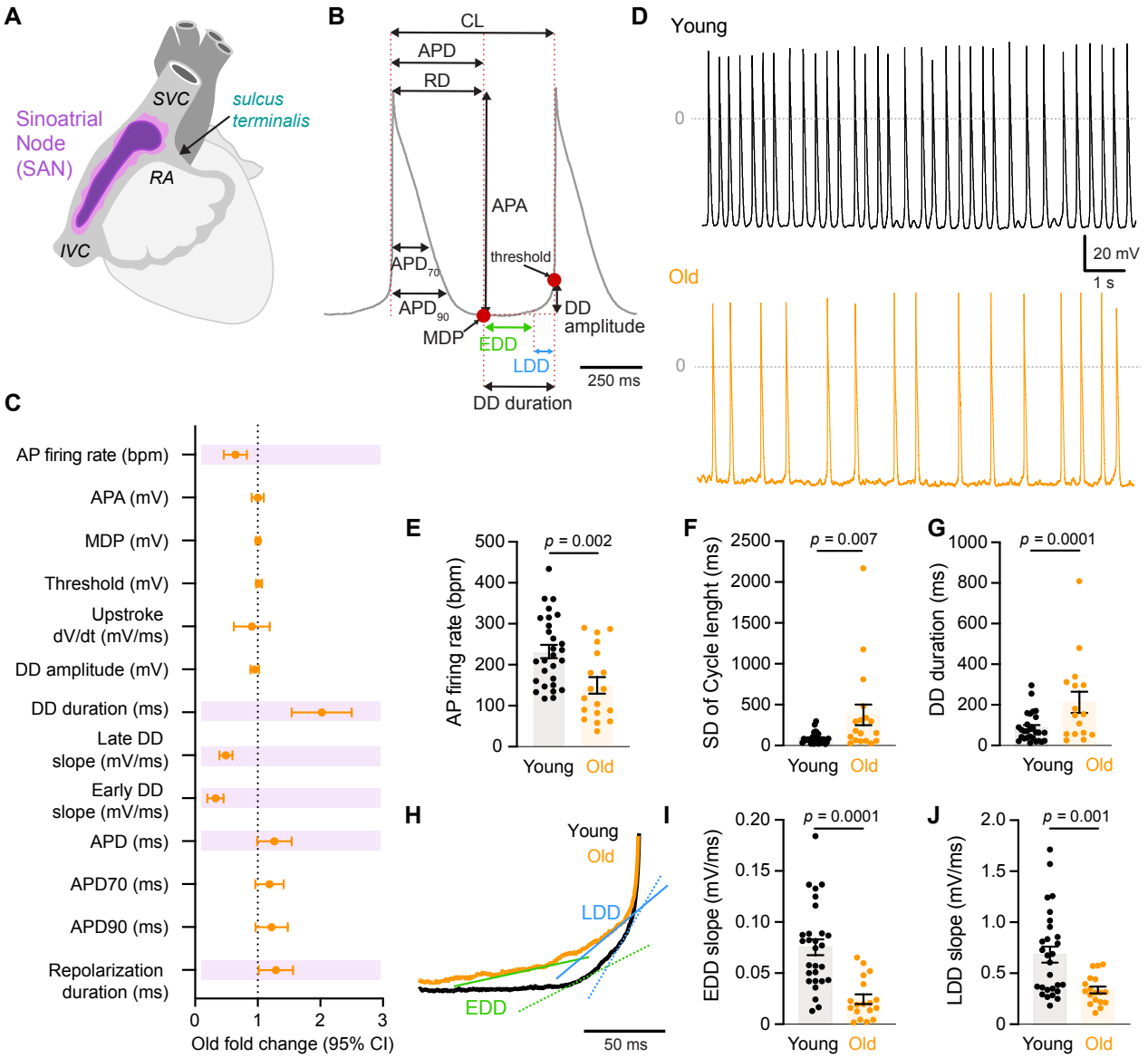

Figure 1. Aging slows down the action potential firing rate and the diastolic depolarization of pacemaker cells. (A) (left) Schematic representation of the position of the sinoatrial node (SAN) pacemaker in the heart located between the right atrium (RA) and the superior and inferior vena cava (SVC, IVC); **(B)** Schematic of two pacemaker action potentials depicting the parameters analyzed (CL: cycle length, APD: action potential duration, RD: repolarization duration, APA: action potential amplitude, MDP: maximum diastolic depolarization, DD: diastolic depolarization, EDD: Early DD, LDD: Late DD. **(C)** Fold change of the action potential parameters analyzed in old pacemaker cells relative to young. Vertical dotted line represents the young population. Purple bars highlight parameters that were significantly different from the young. **(D)** Representative recordings of spontaneous action potential from young (black) and old (orange) pacemaker cells. **(E)** Comparison of the firing rate from young and old pacemaker cells. **(F)** Comparison of the standard deviation (SD) of the cycle length from young and old pacemaker cells. **(G)** Comparison of the DD duration from young and old pacemaker cells. **(H)** Representatives traces of the diastolic depolarization phase from a young and old pacemaker cell to compare the Early DD (green) and Late DD (blue) slopes. Adjusted lines were used to calculate the depolarization rate of each phase. **(I,J)** Comparison of the Early DD and Late DD slopes from young and old pacemaker cells. In all the scattered plots bars represent the mean and error bars the SEM. Statistical comparisons used a two-tail t-test comparing a population of n = 28 cells, N = 5 mice for the young group and n = 18 cells, N = 5 mice for the old.

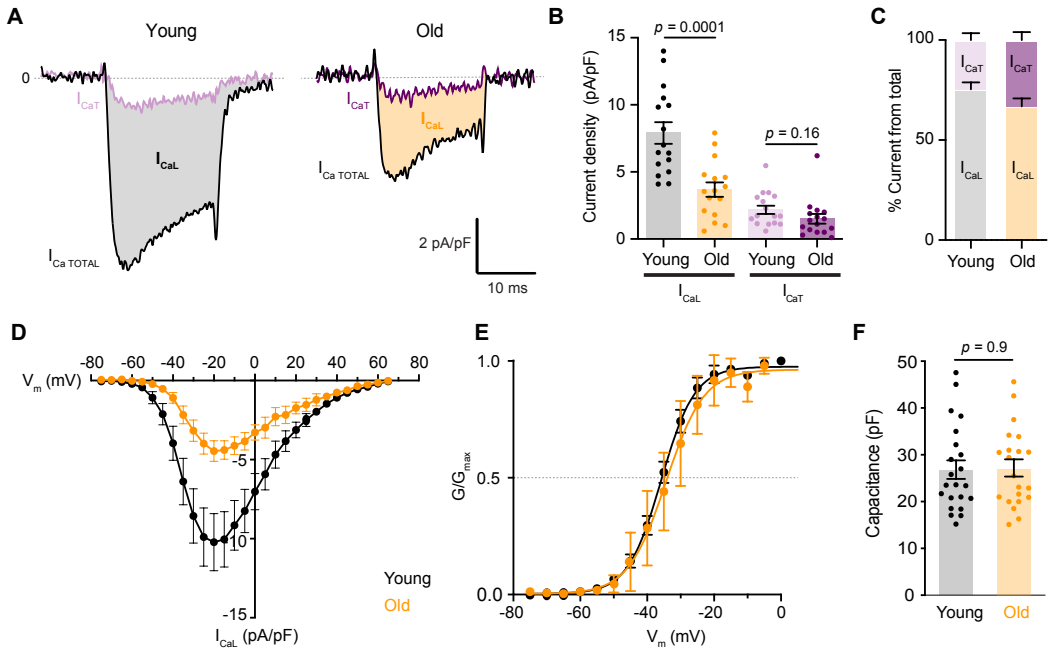

Figure 2. L-type calcium current density is reduced in old pacemaker cells

(A) Representative recordings of the total calcium current ($I_{Ca\ TOTAL}$, black) and the nifedipine-resistant component (I_{CaT}, light and dark purple) from young and old pacemaker cells. Shaded region of the current corresponds to the L-type calcium component (I_{CaL}, grey for young and orange for old) **(B)** Comparison of calcium current density with age for both L- and T-type. **(C)** Comparison of the percentage of the calcium current carried by L- and T-type channels in young versus old cells. **(D)** Comparison of the current-voltage relationship for the L-type calcium current from young and old pacemaker cells. **(E)** L-type conductance G-voltage relationship from young and old pacemaker cells. **(F)** Comparison of the capacitance of young and old pacemaker cells. In all the scattered plots bars represent the mean and error bars the SEM. Statistical comparisons used a two-tail t-test comparing a population of n = 16 cells, N = 4 mice for the young group and n = 16 cells, N = 4 mice for the old, for panels B-E. Panel F sample numbers were n = 22 cells, N = 4 mice for the young group and n = 21 cells, N = 4 mice for the old.

the diastolic depolarization (DD) duration, the slopes of the Early (EDD) and Late (LDD) diastolic depolarization, the action potential duration (APD), and the repolarization duration (Figure 1C). Figure 1D shows representative traces of the spontaneous activity in young and old pacemaker cells. At the population level, action potential firing rate was significantly slower in old cells with a mean ± SEM value of 150 ± 20 bpm compared to 235 ± 16 bpm in young cells (Figure 1E). Action potential firing in old cells had an irregular rhythm evidenced by a higher standard deviation (SD) of the cycle length with a value of 375 ± 127 ms for the old compared to 87 ± 14 ms for the young (Figure 1F). Since the duration and rate of depolarization (i.e. slope) of the DD are key determinants of how fast pacemaker cells can fire, we evaluated the differences between these parameters in young and old cells. Cells from old animals showed a longer DD duration, with an average of 199 ± 24 ms compared to 106 ± 9 ms for the young (Figure 1G). Fitting linear regression equations to the early and late DD, we estimated the change in slope between the two age groups. Figure 1H exemplifies the flattening of the early DD and late DD slopes observed in old pacemaker cells. We found that old cells have a significant reduction in the slopes of both Early DD (young 0.075 ± 0.007 mV/ms vs old 0.024 ± 0.004 mV/ms, Figure 1I) and Late DD (young 0.68 ± 0.08 mV/ms vs old 0.34 ± 0.03 mV/ms, Figure 1J). Pacemaker cells from old animals also exhibited significant increases in the action potential duration (young 144 ± 9 ms vs old 183 ± 19 ms).

L-type calcium current density is reduced in old pacemaker cells

The flattening of the DD observed in pacemaker cells from old animals suggests that aging has a direct effect on the ion channels responsible for this spontaneous depolarization. Given the proposed role of L-type calcium channels in the DD, we sought to determine whether isolated pacemaker cells from old animals had differences in their calcium current density. Whole-cell calcium currents were recorded from isolated pacemaker cells in response to 20 ms depolarizing pulses to -20 mV from a holding potential of -80 mV. Figure 2A shows representative traces of the total calcium current ($I_{Ca\ TOTAL}$) in young and old pacemaker cells. To isolate the L-type calcium component, calcium currents were blocked bathing the cells with an external solution containing 10 μM of specific L-type blocker nifedipine. As it can be seen in the light and dark purple traces in Figure 2A, only a small component of the $I_{Ca\ TOTAL}$ is resistant to nifedipine and carried by T-type calcium channels (I_{CaT}). The L-type component of the current (I_{CaL}) was calculated by subtracting the nifedipine-resistant component from the $I_{Ca\ TOTAL}$. The analysis of the I_{CaL} and I_{CaT} current densities showed that aging reduced specifically the I_{CaL}, going from 7.9 ± 0.8 pA/pF in young cells to 3.7 ± 0.5 pA/pF in the old (Figure 2B). In contrast, I_{CaT} was not significantly different with values of 2.2 ± 0.3 pA/pF in young cells and 1.5 ± 0.4 pA/pF in old. Aging did not alter either the percentage of the $I_{Ca\ TOTAL}$ carried by L-type or T-type calcium channels (Figure 2C). In young pacemaker cells, 75 ± 4% of the calcium current was carried by L-type and 25 ± 4% by T-type channels. Similarly, in old pacemaker cells 67 ± 4% of the calcium current was carried by L-type and 33 ± 4% by T-type channels. We also evaluated the effect of aging on the voltage dependence of the L-type calcium current. For this, we constructed I-V and G-V L-type calcium currents curves in response to increasing 5 mV depolarizing pulses from a holding potential of -75 mV to +65 mV. Old pacemaker cells had a significant reduction of the L-type calcium current at all voltages with no shift of the voltage dependence (Figures 2D, 2E). We did not observe any changes in membrane capacitance between young and old cells (Figure 2F), ruling out that the observed current reduction is due to cell hypertrophy.

Reduction in L-type calcium current in old pacemaker cells is associated with a decrease in their expression and clustering at the plasma membrane

To evaluate if the observed age-associated reduction in current density was caused by a reduction in the L-type calcium channel abundance, we measured the protein levels by western blot from protein lysates obtained from entire sinoatrial node explants from young and old animals. Protein levels for $Ca_V1.2$ were 1.9 ± 0.4-fold higher in old animals compared to the young. In contrast, $Ca_V1.3$ expression was unchanged in old animals with a value of 0.9 ± 0.2-fold relative to the young (Figures 3A and 3B). Then, we evaluated if aging affected the expression of the $Ca_V1.2$ and $Ca_V1.3$ channels at the plasma membrane by measuring the density of the channels detected with immunocytochemistry in isolated cells using high-resolution AiryScan microscopy at the focal plane of the footprint of the cells. We observed that old cells showed 19% fewer $Ca_V1.2$ particles per membrane area, with a density of 0.54 ± 0.03 particles/μm^2 compared to 0.67 ± 0.05 particles/μm^2 in the young (Figures 3C, 3D, and 3G). $Ca_V1.3$ particle density was reduced in old pacemaker cells by 24%, with values of 0.75 ± 0.03 particles/μm^2 for the young and 0.58 ± 0.03 particles/μm^2 for the old (Figures 3E, 3F, and 3G).

We have previously shown that L-type $Ca_V1.2$ and $Ca_V1.3$ channels organize in packed clusters at the plasma membrane in several cell types, including ventricular cardiomyocytes and hippocampal neurons ***Dixon et al.*** (***2015***); ***Moreno et al.*** (***2016***); ***Del Villar et al.*** (***2021***); ***Ghosh et al.*** (***2018***). More importantly, we have shown that this clustering is essential for L-type calcium channels to undergo a functional coupling that increases their open probability. Hence, we assessed whether the decrease in channel density at the plasma membrane observed in old cells correlates with a disruption in channel clustering. Using Ground-State Depletion super-resolution microscopy, we imaged young and old pacemaker cells immunostained against $Ca_V1.2$ and $Ca_V1.3$ channels .

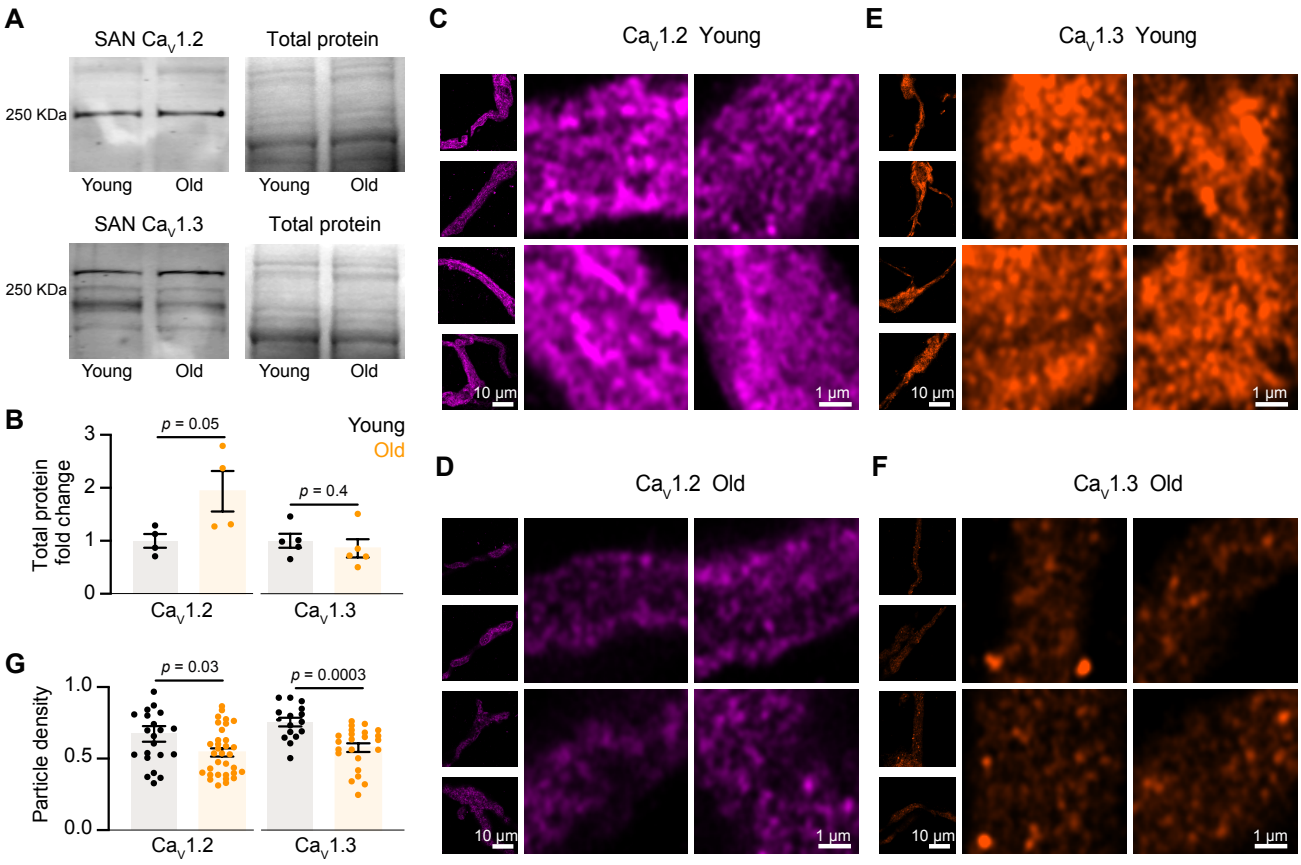

Figure 3. Aging does not affect the total expression of L-type calcium channels but reduces their density at the plasma membrane
(A) Representative western blots for $Ca_V1.2$ and $Ca_V1.3$ channels and total protein stains from pacemaker tissue explants from young and old mice.**(B)** Fold change of $Ca_V1.2$ and $Ca_V1.3$ channel total expression in old animals relative to young. Expression was normalized to total protein and each data point represents an animal. Statistical comparisons used a two-tail Mann-Whitney test. **(C-F)** Small insets to the right are representative AiryScan high-resolution images of the footprint of young and old pacemaker cells labeled against $Ca_V1.2$ (magenta) or $Ca_V1.3$ (orange). Magnified panels to the left are 5 by 5 µm footprint regions from each of the cells shown to the right. **(G)** Comparison of $Ca_V1.2$ and $Ca_V1.3$ particle density between young ($Ca_V1.2$, n = 22, N = 3; $Ca_V1.3$, n = 16, N = 3) and old ($Ca_V1.2$, n= 33, N = 3; $Ca_V1.3$, n = 23, N = 3) cells. Statistical comparisons used a two-tail t-test.

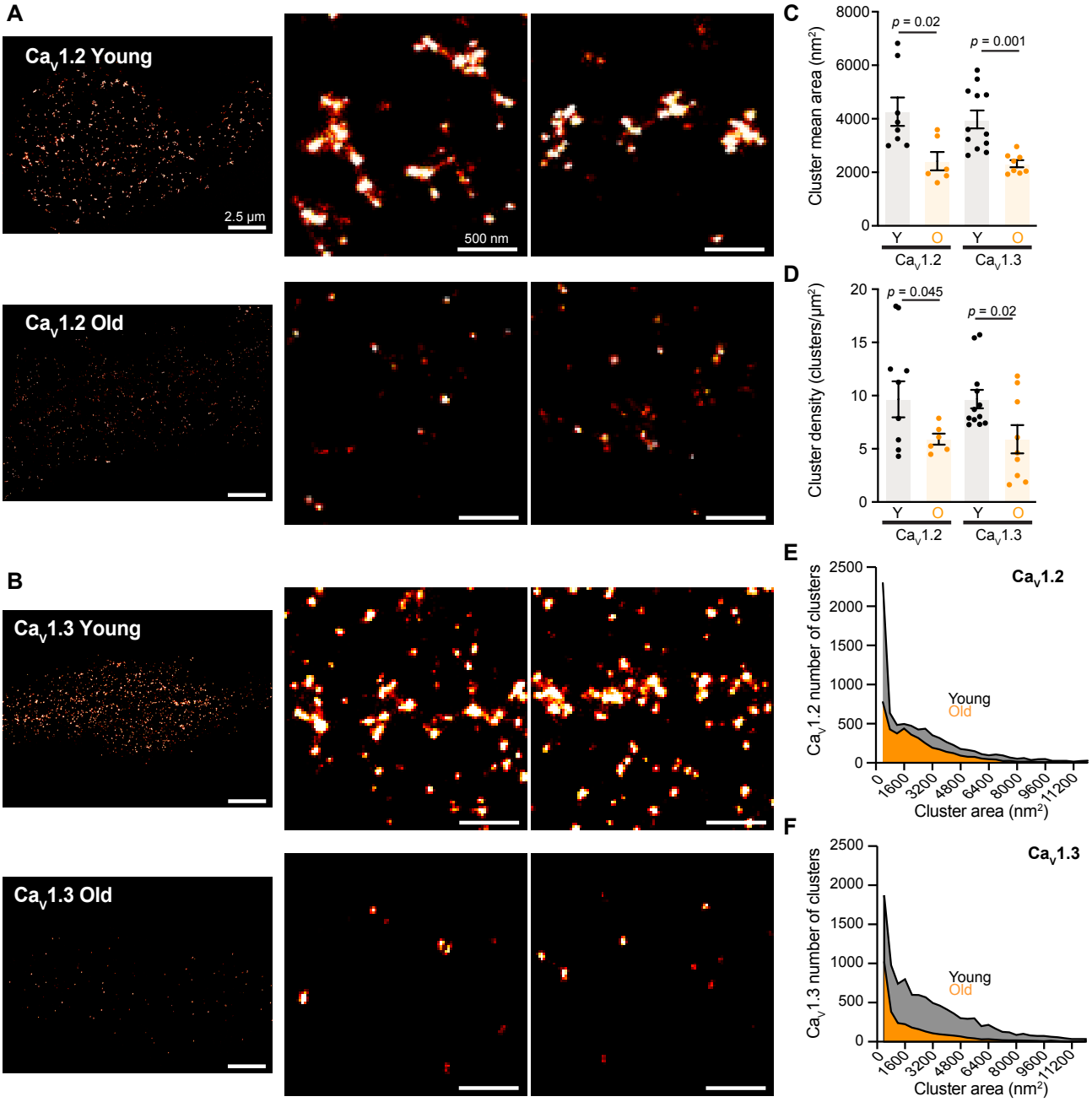

Figure 4. Aging reduces L-type calcium channel clustering

(A, B) Representative super-resolution (GSD) images of $Ca_V1.2$ and $Ca_V1.3$ channels in young and old pacemaker cells. Panels to the right of each image are zoom in. **(C)** Average cluster area for $Ca_V1.2$ and $Ca_V1.3$ channel clusters in young and old pacemaker cells. **(D)** Comparison of $Ca_V1.2$ and $Ca_V1.3$ cluster density between young and old cells. **(E,F)** Comparison of the frequency distributions of the area of $Ca_V1.2$ and $Ca_V1.3$ channel clusters between young and old cells. In all the scattered plots bars represent the mean and error bars the SEM. Statistical comparisons used a two-tail t-test comparing a population of n = 8 cells, N = 3 mice for $Ca_V1.2$ young; n = 12 cells, N = 4 mice for $Ca_V1.3$ young; n = 6 cells, N = 3 mice for $Ca_V1.2$ old; and n = 8 cells, N = 3 mice for $Ca_V1.3$ old.

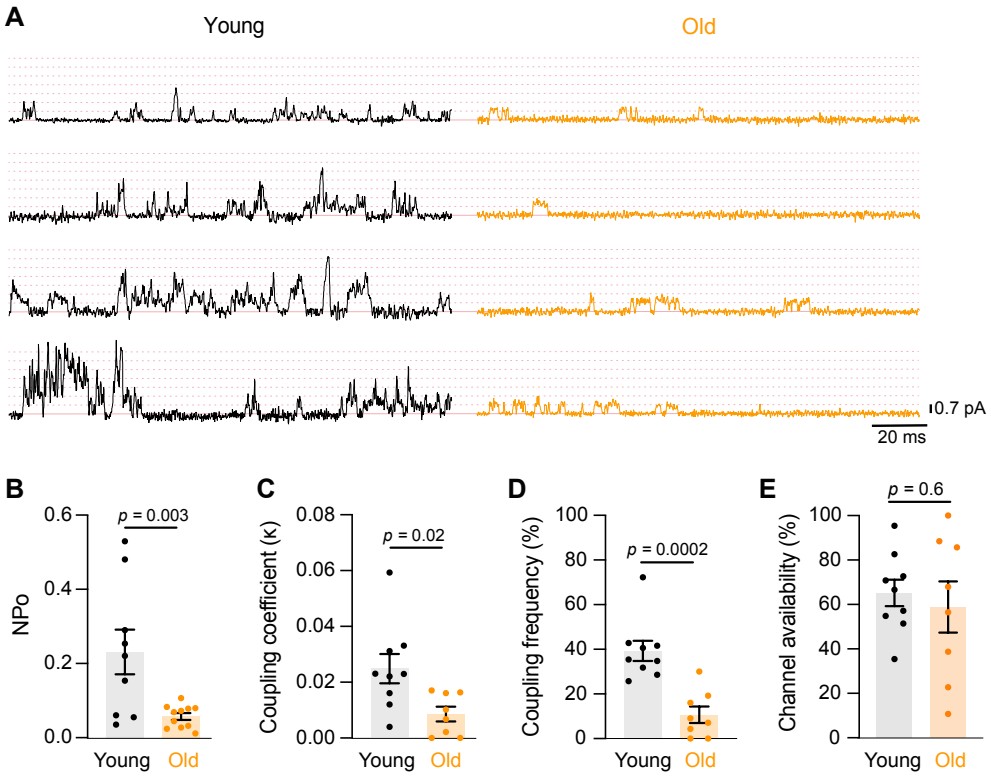

Figure 5. Aging reduces L-type calcium channel open probability and coupling coefficient
(A) Representative single-channel recordings from young (black) and old (orange) pacemaker cells. Dotted lines represent number of channels opening (1-7 channels), from the baseline closed state based on a unitary current of 0.7 pA. **(B)** Comparison of the channel open probability (NP_O) between young and old pacemaker cells calculated from 50 voltage sweeps per cell. **(C)** Comparison of the coupling coefficient (κ) between young and old pacemaker cells. **(D)** Comparison of the percentage of coupling frequency between young and old pacemaker cells. **(E)** Comparison of the percentage of channel availability between young and old pacemaker cells. In all the scattered plots bars represent the mean and error bars the SEM. Statistical comparisons used a two-tail t-test comparing a population of n = 9 cells, N = 3 mice for the young group and n = 8 cells, N = 3 mice for the old group.

We found that in young pacemaker cells, both L-type calcium channels organize in clusters at the plasma membrane with an average size of 4265 ± 531 nm^2 for the $Ca_V1.2$ and 3975 ± 334 nm^2 for the $Ca_V1.3$ (Figures 4A, 4B, and 4C). Cells from old animals showed a significant reduction in the mean cluster area with values of 2416 ± 342 nm^2 for $Ca_V1.2$, and 2321 ± 132 nm^2 for $Ca_V1.3$ channels (Figures 4A, 4B, and 4C). An analysis of the cluster density of the channels showed an age-associated significant reduction for both channels. For the $Ca_V1.2$ channels, cluster density went from 9.6 ± 1.7 clusters/μm^2 in young cells to 5.9 ± 0.5 clusters/μm^2 in the old (Figure 4D). For $Ca_V1.3$ channels, cluster density went from 9.7 ± 0.9 clusters/μm^2 in young to 5.9 ± 1.3 clusters/μm^2 in old cells (Figure 4D). Figures 4E and 4F show the frequency distribution for the $Ca_V1.2$ and $Ca_V1.3$ channel cluster area. The distributions were in both cases shifted to the left in old cells, suggesting an age-associated global reduction in the L-type channel cluster size. Interestingly, a more pronounced reduction in cluster size was observed for the $Ca_V1.3$ channel and this was observed not only at the 20 nm resolution level of the GSD but was even evident at the 120 nm resolution of the Airyscan analysis.

L-type calcium channel open probability and channel coupling coefficient are reduced in old pacemaker cells

$Ca_V1.2$ and $Ca_V1.3$ channels undergo a functional physical coupling through their C-terminals that results in an increase in channel open probability. We have previously shown that this coupled gating mechanism increases firing rate in neurons ***Moreno et al.*** (***2016***). Clustering is required for the functional coupling of L-type calcium channels to occur. Given the observed age-associated reduction in L-type calcium channel clustering in old pacemaker cells, we evaluated if they also exhibited a reduction in the open probability and the coupling of calcium channels. For this, we measured single-channel activity in isolated pacemaker cells from young and old cells in the cell-attached configuration. Figure 5A shows representative single-channel recordings from young and old pacemaker cells in response to 200 ms depolarizing pulses at -20 mV. We did not restrict our analysis to patches containing one single channel, since the main goal of this experiment was to evaluate the coupled opening of the channels. Single-channel records in young pacemaker cells were characterized for the coordinated opening of multiple channels while in old cells unitary and independent single-channel events were predominant (Figure 5A). The analysis of the open probability (NP_O) showed that calcium channels in old cells had a 4-times lower NP_O (0.06 ± 0.01) compared to young cells (0.23 ± 0.06) (Figure 5B). To evaluate if aging was affecting in a similar way the coupling of these channels, we calculated the coupling coefficient (κ) from these traces using a coupled Markov-chain model following the method by Chung and Kennedy, 1996 ***Chung and Kennedy*** (***1996***). The coupling coefficient (κ) is a dimensionless value ranging between 0 and 1, where 0 corresponds to fully uncoupled channels and 1 to fully coupled channels. Using this approach, we found that the coupling coefficient in old pacemaker cells was reduced from a value of 0.025 ± 0.005 in young to 0.009 ± 0.003 in old cells (Figure 5C). Coupling frequency was calculated as the percentage of sweeps from a cell with (κ) > 0. Old pacemaker cells showed a coupling frequency of 11 ± 4%, significantly lower than the coupling frequency of 39 ± 5% observed in young cells (Figure 5D). We quantified as well channel availability, as the percentage of sweeps showing channel openings regardless of their coupling coefficient. Channel availability was not significantly different between the two groups, with values of 65 ± 6% for young cells and 59 ± 11% for old cells (Figure 5E), suggesting that the observed reduction in coupling frequency in old cells was not due to a higher frequency of sweeps without channel activity. Together, these results support the hypothesis that calcium channels have a reduced coupled gating in old pacemaker cells causing a decrease in their open probability.

Increasing L-type calcium channel open probability restores firing rates in pacemaker cells from old animals

We tested further our working hypothesis by asking if increasing the open probability of L-type calcium channels could reverse the age-associated slowdown of the pacemaker. To test this, we recorded the spontaneous firing rate of isolated young and old pacemaker cells in control conditions and under the bath application of 500 nM of the L-type channel agonist Bay K 8644. Bay K has been shown to increase the open probability and opening time of L-type calcium channels ***Bechem and Schramm*** (***1987***); ***Brown et al.*** (***1984***); ***Hess et al.*** (***1984***); ***Kokubun and Reuter*** (***1984***); ***Thomas et al.*** (***1985***); ***Zhao et al.*** (***2019***). In this new experimental set under control conditions, we found that rate was slower in cells from old animals compared to young, as we had shown before (Figure 6A, left). The perfusion of Bay K accelerated the spontaneous firing rate in young cells 1.3-fold, going from 209 ± 22 bpm to 283 ± 20 bpm (Figure 6B). The effect of Bay K in old cells was stronger, with an acceleration of 1.6-fold, going from 151 ± 27 to 242 ± 19 bpm (Figures 6A and 6B). Remarkably, increasing L-type calcium channel open probability with Bay K was enough to accelerate firing rate in old cells to values not significantly different from the young group (Figure 6B). Increasing the open probability of L-type calcium channels had a similar effect on other parameters of the action potential. The application of Bay K reverted the significant differences observed in control

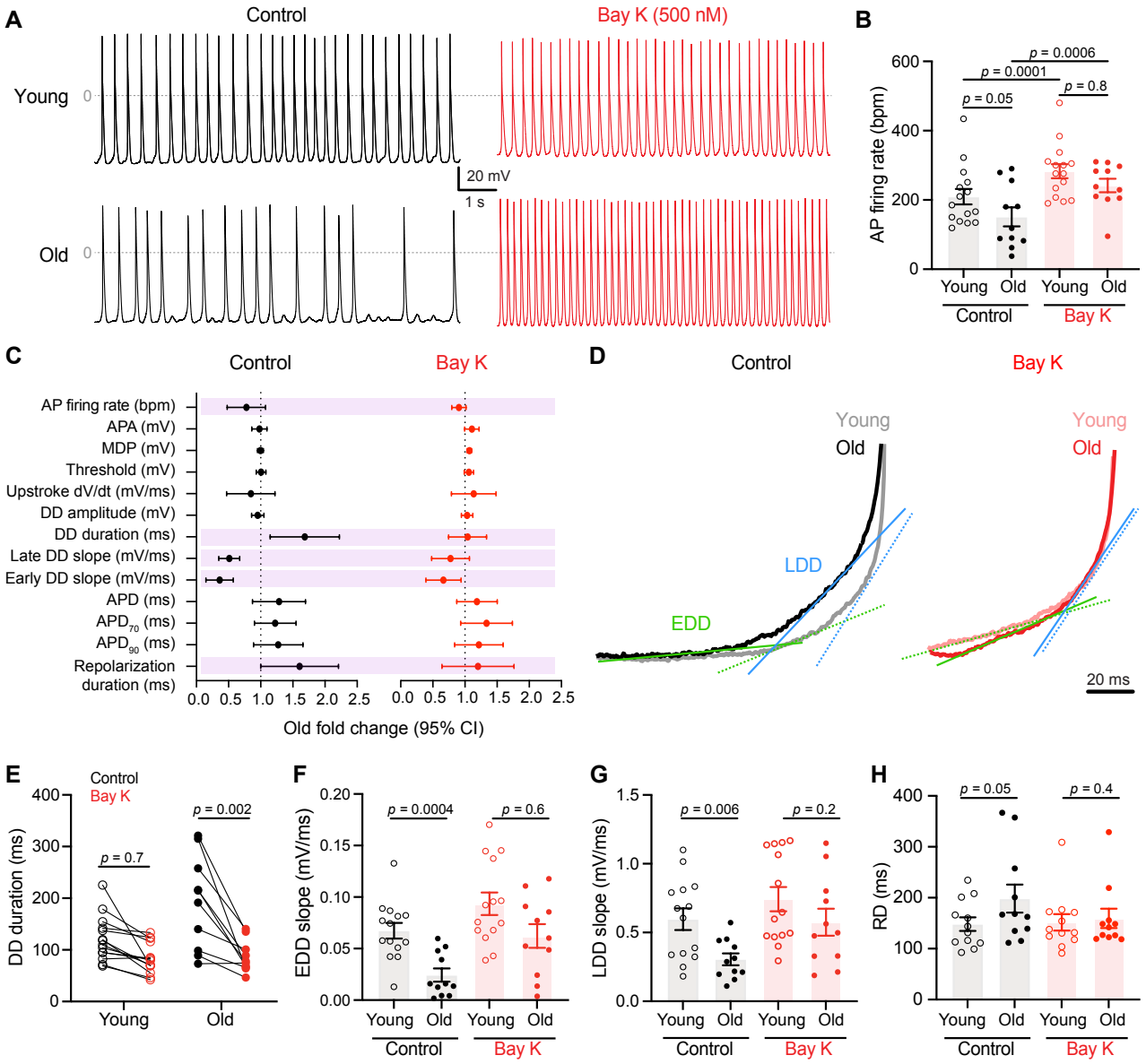

Figure 6. Increasing L-type calcium channel open probability restores normal pacemaking rates in old cells

(A) Representative recordings of action potentials from young and old pacemaker cells before (black) and after (red) application of 500 nM Bay K8644. **(B)** Comparison of the effect of Bay K on the firing rate of young and old pacemaker cells. **(C)** Fold change of the action potential parameters analyzed in old pacemaker cells relative to young in control (black) and Bay K (red). Vertical dotted lines represents the young population. Purple bars highlight parameters that were significantly different in control conditions but reverted by Bay K. **(D)** Representative overlapped magnification of the diastolic depolarization in the absence (control) and presence of Bay K. Straight lines illustrate how the kinetics of the Early DD (green) and Late DD (blue) phases were calculated from young (dotted) and old (solid) traces. **(E)** Comparison of the effect of Bay K (red) on the duration of the diastolic depolarization (DD) relative to control (black) in young and old pacemaker cells. **(F, G)** Comparison of the slopes of the tangential lines for Early DD (F) and Late DD (G) between young and old pacemaker cells in control conditions (black) and upon the subsequent addition of Bay K (red). **(H)** Comparison of the repolarization duration (RD) between young and old pacemaker cells in control conditions (black) and upon the subsequent addition of Bay K (red). In all the scattered plots bars represent the mean and error bars the SEM. Statistical comparisons between young and old used a two-tail t-test comparing a population of n = 14 cells, N = 3 for the young and n = 11 cells, N = 3 mice for the old. Statistical comparisons between control and Bay K used a paired two-tail t-test.

conditions between young and old for the DD duration, Early DD and Late DD slopes, and in the repolarization duration (Figure 6C). Given the slowdown of the Early DD and Late DD in old cells shown in Figure 1, we analyzed the effect of Bay K on the DD duration and on the slopes of the Early and Late DD. Bay K changed the kinetics of Early DD and Late DD in old cells making them similar to those observed in the young (Figure 6D). A paired analysis of the DD showed that Bay K shortened significantly DD only in old cells (Figure 6E). Bay K induced a significant increase in the slope of the Late DD and Early DD in both groups (Figures 6F and 6G). In control conditions, the Early DD and Late DD slopes were significantly less steep in old cells when compared to the young (Early DD: 0.02 ± 0.1 mV/ms in old vs 0.07 ± 0.01 mV/ms in young; Late DD: 0.30 ± 0.04 mV/ms in old vs 0.60 ± 0.08 mV/ms in young) (Figures 6F and 6G). However, under Bay K application, Early DD and Late DD were significantly accelerated in the old group reverting the significant differences relative to the young (Early DD: 0.09 ± 0.01 mV/ms in young vs 0.06 ± 0.01 mV/ms in old; Late DD: 0.74 ± 0.09 mV/ms in young vs 0.58 ± 0.01 mV/ms in old cells and). Early DD and Late DD were accelerated 1.4 and 1.2 times, respectively in young cells. In contrast, in old cells Bay K accelerated Early DD 2.6 times and Late DD 1.9 times. The differences in the repolarization time were also reverted upon Bay K treatment (Figure 6H). Together, these results suggest that increasing the open probability of L-type calcium channels in old pacemaker cells contributes to pacemaker rate acceleration through an increase in the diastolic depolarization rate combined with a reduction in the time for repolarization.

Discussion

Cardiac pacemaker cells drive heart rhythm and depend on L-type calcium channels to do it. Pacemaker firing rate declines linearly with age but the molecular mechanisms of this slowdown are not completely understood. Our findings demonstrate that aging alters the spatial organization and activity of L-type calcium channels. Pacemaker cells from old animals exhibit a reduction in L-type calcium channel clustering accompanied by a reduction in their coupling coefficient and in their open probability. These age-associated alterations in activity of L-type calcium channels result in a significant net reduction of I_{CaL} in old pacemaker cells. This leads to a slowing of the Early DD and Late DD phases, increasing the latency between consecutive action potentials. Interestingly, we found that increasing the open probability of L-type calcium channels pharmacologically is enough to restore firing rates in old pacemaker cells to those values observed in the young. This study provides physiological evidence of the effect of aging on the activity of L-type calcium channels. Our evidence favors the model in which alterations in the intrinsic electric properties of pacemaker cells is a key determinant for their age-associated dysfunction.

The remodeling of ionic currents, including the down-regulation or up-regulation of the expression of specific ion channels, has been proposed to be one of the main mechanisms underlying the age-associated dysfunction of the cardiac pacemaker ***Huang et al.*** (***2015***, 2016); ***Peters et al.*** (***2020***); ***Tellez et al.*** (***2011***). Interestingly, a recent in silico model ***Alghamdi et al.*** (***2020***) concluded that while an integral remodeling of ion channels and calcium handling proteins occurs in the aged pacemaker, the remodeling of I_{CaL}, either via a gain or loss of function, is the most significant factor underlying the slowing down of pacemaking rates in old animals. Age-associated changes in L-type calcium channel expression have been little studied in pacemaker cells and a consensus of the effect has not yet been reached. Tellez et al. found a discrete increase in $Ca_V1.2$ at the mRNA level in the aged rat pacemaker ***Tellez et al.*** (***2011***). In contrast, at the protein level, the expression of $Ca_V1.2$ channels in the pacemaker has been reported to be reduced by about 40% in aged rats ***Hatch*** (***2012***) and by almost 80% in aged guinea pigs ***Jones et al.*** (***2007***). Age-associated changes in the expression of $Ca_V1.3$ channels have been even less explored and no differences at the mRNA level have been found between young and old pacemakers ***Tellez et al.*** (***2011***). Our results show that, in the mouse pacemaker, aging alters in a different way the total protein levels of the $Ca_V1.2$ and the $Ca_V1.3$ channels. While $Ca_V1.2$ protein abundance was increased in old animals, $Ca_V1.3$ re-

mained unchanged. Given that $Ca_V1.3$ channels are exclusively expressed in the pacemaker and in the heart's conduction system while $Ca_V1.2$ channels are ubiquitously expressed in the heart, this suggests that the transcription and translation of these channels are regulated in a different manner in the pacemaker tissue. However, we found that aging reduced the cluster density of both channels at the plasma membrane, suggesting that the mechanisms behind the trafficking and insertion of the channels might be the same. Many of the studies designed to identify the mechanisms behind the age-associated alterations of ionic currents have focused on the role of aging in regulating ion channel expression ***Huang et al.*** (***2015***, 2016); ***Peters et al.*** (***2020***); ***Tellez et al.*** (***2011***). Our results open a new scenario in which the effects of aging on other factors including trafficking, plasma membrane insertion, scaffolding, turnover, and membrane organization of ion channels, need to be taken into account. One of the limitations of our study is that, given the lack of specific inhibitors to separate the $Ca_V1.2$ and the $Ca_V1.3$ currents, we cannot determine if the effects of aging on the single channel activity, open probability, and channel cooperativity differ between both channels. However, given the different role that both channels play in the pacemaking mechanisms, with $Ca_V1.3$ channels involved in the DD and $Ca_V1.2$ channels involved in the action potential upstroke, our results suggest that that is the case. Aging increased significantly DD duration and reduced its rate but had no effect on the upstroke (dV/dT).

How does aging reduce the clustering of calcium channels? In contrast to working cardiomyocytes, pacemaker cells lack T-tubules. However, they have an extensive caveolar network that serves as specialized signaling microdomains where many channels, including L-type calcium channels, reside. We have recently shown in pacemaker cells that aging causes a reduction in caveolae density accompanied by a decrease in the proximity of $Ca_V1.2$ and $Ca_V1.3$ channels to caveolin-3 ***Choi et al.*** (***2022***). Although the molecular mechanism mediating L-type calcium channel clustering has not been identified yet, a reduction in the availability of these specialized caveolar microdomains could decrease the insertion and proximity between L-type calcium channels. Another factor contributing to a loss of clustering could be alterations in the expression and function of scaffolding proteins. Scaffolds identified to bind L-type calcium channels in other cell types include BIN1 ***Hong et al.*** (***2012***, 2010), AKAPs ***Altier et al.*** (***2002***); ***Davare et al.*** (***1999***); ***Gao et al.*** (***1997***); ***Marshall et al.*** (***2011***); ***Nystoriak et al.*** (***2017***), and Shank ***Olson et al.*** (***2005***); ***Pym et al.*** (***2017***); ***Zhang et al.*** (***2005***). BIN1 plays an important role in the delivery and clustering of $Ca_V1.2$ channels in ventricular cardiomyocytes, while AKAP150 has been shown to be necessary for the cooperative gating of $Ca_V1.2$ channels in smooth muscle cells. However, the function of the majority of these scaffolds remains to be tested in pacemaker cells. We recently showed that AKAP150 associates to $Ca_V1.2$ and $Ca_V1.3$ channels in pacemaker cells and that aging abolishes this interaction almost completely ***Choi et al.*** (***2022***). More studies are needed to understand how aging alters the delivery and scaffolding of L-type calcium channels and other ion channels and the formation and maintenance of functional signaling microdomains at the plasma membrane.

Here we showed that firing rate in old pacemaker cells could be boosted to those levels observed in the young by pharmacologically increasing L-type calcium channel open probability. This finding suggests that old pacemaker cells have in their membranes a population of L-type channels operating in a low open probability mode that can be recruited to increase calcium entry. Navedo et al. have shown that L-type calcium channels can in fact operate in either low or high open probability modes in smooth muscle cells ***Amberg et al.*** (***2007***). The age-associated reduction in channel clustering that we reported, could be a factor altering the number of quiet channels in pacemaker cells. Why the observed increase in firing rate upon Bay K application is not linear between young and old is an interesting question that could be explained by different proportions of these quiet channels that can be potentiated. Also, there are other limiting factors that set a maximum firing rate at which both, young and old cells, can fire. Thus, the initial slower firing of old cells gives a broader window of action to see the effect of calcium channel potentiation, before that limit is reached. Other important factors that can modulate calcium channel activity include the action

of the accessory β and $\gamma\delta$ subunits that can regulate the trafficking and the insertion of the channels into the membrane ***Dolphin*** (***2012***), or the association with small GTPases like Rad, that can directly inhibit the calcium channel ***Finlin et al.*** (***2003***); ***Liu et al.*** (***2020***); ***Magyar et al.*** (***2012***); ***Papa et al.*** (***2021***); ***Xu et al.*** (***2010***). How aging affects these opposite modulatory proteins still needs to be evaluated.

As Bertil Hille states in his classic book, cardiac pacemaking is a quasi-equilibrium process driven by the minuscule imbalance of much larger component currents ***Hille*** (***2001***). Thus, even the smallest change in any of its components can alter dramatically pacemaker rate. A good example of this is the fact that for many years it was thought that the spontaneous DD phase that confers automaticity to the pacemaker was sustained only by the funny current carried by HCN4 channels. Surprisingly, $Ca_V1.3^{-/-}$ KO mice exhibited a striking bradycardia ***Mangoni et al.*** (***2003***); ***Platzer et al.*** (***2000***), unveiling the important role of $Ca_V1.3$ channels in the firing rate of pacemaker cells, despite the small amount of current flowing through these channels at these negative potentials. More recently, it has been shown that localized entry of calcium through $Ca_V1.3$ channels also plays an important role in the synchronization of local calcium release through ryanodine-receptors type 2 (RyR2) during the Early DD ***Torrente et al.*** (***2016***); ***Wang et al.*** (***2017***); ***Arbel-Ganon et al.*** (***2020***), functioning as an amplifying mechanism that contributes to the spontaneous depolarization. Our results showing that increasing the open probability of L-type calcium channels with Bay K accelerates both, the Early and the Late DD phases, highlights the interconnectivity of these processes. Thus, the answer to the question of how aging alters the pacemaking mechanism has to take into account the intricated interconnected nature of the pacemaking. Proenza et al. have provided so far enough evidence showing that aging causes a hyperpolarizing shift in the voltage dependence of activation of HCN4 channels that contributes to the slowdown of the pacemaker ***Larson et al.*** (***2013***); ***Sharpe et al.*** (***2017***). In this study, we provide evidence of how aging reduces significantly one of this components, the L-type calcium current. How these changes are engrained still needs to be studied. Finally, our observations provide evidence that aging is impacting the function and modulation of ion channels, sparking new questions on how age-associated alterations in cell excitability contribute to the aging process and can underlie many of its associated pathologies.

Methods and Materials

Solutions

For the isolation of pacemaker cells, the following solutions were used: Tyrode's III solution (in mM) – 148 NaCl, 5.4 KCl, 5 HEPES, 5.5 glucose, 1 $MgCl_2$, and 1.8 $CaCl_2$, pH was adjusted to 7.4 with NaOH. Low-Calcium Tyrode's solution (in mM) – 140 NaCl, 5.4 KCl, 5 HEPES, 5.5 glucose, 1.2 KH_2PO_4, 50 taurine, 0.5 $MgCl_2$, and 0.2 $CaCl_2$, pH was adjusted to pH 6.9 with NaOH. KB solution (in mM) – 80 L-glutamic acid, 25 KCl, 10 HEPES, 10 glucose, 10 KH_2PO_4, 20 taurine, 0.5 EGTA, and 3 $MgCl_2$, pH was adjusted to 7.4 with KOH.

For electrophysiological recordings, the following solutions were used: Whole-cell voltage-clamp calcium current (ICa) external solution (in mM) – 110 N-methyl-D-glutamine, 5 CsCl, 10 HEPES, 10 glucose, 30 TEA-Cl, 4 4-Aminopyridine, 1 MgCl2, and 2 CaCl2, pH was adjusted to 7.4 with HCl. I_{Ca} internal solution (in mM) – 50 CsCl, 10 HEPES, 70 L-Aspartic acid, 30 TEA-Cl, 5 EGTA, 5 Mg-ATP, 1 $MgCl_2$, and 0.7 $CaCl_2$, pH was adjusted to 7.2 with CsOH. Perforated-patch current-clamp action potential external solution was Tyrode's III. Perforated-patch current-clamp action potential internal solution (in mM) – 130 L-Aspartic acid K, 10 NaCl, 10 HEPES, 0.04 $CaCl_2$, 2 Mg-ATP, 0.1 Na-GTP, 6.6 phosphocreatine, pH was adjusted to 7.2 with KOH. On the day of the experiment, freshly prepared β-Escin was added to the intracellular solution to reach a final concentration of 25 µM. Cell-attached single channel recording external solution (in mM) – 145 KCl, 10 NaCl, 10 HEPES, pH was adjusted to 7.4 with NaOH. Cell-attached single channel recording internal solution (in mM) – 110 $CaCl_2$, 20

TEA-Cl, 10 HEPES, and 10 μM of the HCN channel-blocker ivabradine, pH was adjusted to 7.2 with CsOH.

For protein extraction, the following solutions were used: Homogenization buffer (in mM) – 150 NaCl, 50 Trizma base (from 1M stock at pH 7.8 with HCl), 5 EDTA (from 50 mM stock pH 7.8 with NaOH); the day before the experiment NaF 10 mM, Glycerol 5% v/v, Triton X-100 1% v/v, Sodium deoxycholate 0.25% were added; on the day of the experiment one tablet of SIGMAFAST$_{TM}$ protease inhibitor cocktail (Sigma, S8830), EDTA free in 50 ml of the buffer was added. Lysis Buffer (to make 10 ml) – 10 ml of homogenization buffer, 8.3 μl Calpain I (10 mg/ml) (Fisher, AAJ61766LB0), 8.3 μl Calpain II (10 mg/ml) (Sigma, A6060), 10 μl o-phenathroline (200 mg/ml) (Sigma, 33510), 10 μl PMSF (20 mg/ml) (Sigma, P7626), 10 μl Benzamidine (15.7 mg/ml) (Sigma, 12072), prepared the day of the experiment. Solutions were kept on ice.

Pacemaker cells isolation

Pacemaker cells were freshly isolated from mature adults (4-6 months-old), or old (24-28 months-old) C57BL/6 male mice. All work with animals was performed under an approved protocol by the University of Washington Institutional Animal Care and Use Committee (IACUC). Animals were euthanized by intraperitoneal overdose of Euthasol (Virbac, 400mg/ml). The heart was dissected and pinned down on a Sylgard-coated dish containing warm Tyrode's III solution. The sinoatrial node region was identified under the stereoscope as the region delimited at the top by the superior vena cava, at the right by the sulcus terminalis, and at the bottom by the coronary sulcus and the inferior vena cava (Figure 1A). Additionally, the sinoatrial node artery was used as an anatomical landmark to identify the pacemaker region. Pacemaker cells were then isolated from the sinoatrial node following the protocol described by Fenske et al. 2016 ***Fenske et al.*** (***2016***). Briefly, the excised sinoatrial node tissue was immersed into a 37°C pre-heated 2 mL tube containing 675 μl of Low-Calcium Tyrode's. After 5 min of stabilization at 37°C the following compounds were added to the tube: BSA (Cf = 1 mg/ml), elastase (Cf = 18.87 U/ml, Millipore 324682), protease (Cf = 1.79 U/ml, Sigma P5147), and collagenase B (Cf = 0.54 U/ml, Roche 11088807001). The enzymatic digestion of the tissue was carried out for 30 min in a 37°C water bath, a mechanical dissociation with a short fire-polished glass pipette was performed every 10 min during incubation. To stop the digestion, the digested tissue was centrifuged at 200 rfc for 2 min at 4°C, and the supernatant was discarded and replaced with 1 ml of Tyrode's Low-Ca2+ solution, this process was repeated twice. Then the tissue was washed two times more with 1 ml of Calcium-free KB solution. The dissociated tissue was left to rest in KB solution at 4°C for a minimum of 40 min. Finally single pacemaker cells were resuspended applying gentle mechanical dissociation with a flame-forged glass pipette. For electrophysiology experiments, to recover the automaticity of the pacemaker cells, calcium was reintroduced into the KB cell's storage solution by the gradual addition of small amounts of Tyrode's III solution (10, 50 and 100 μl at 5 min intervals). Cells were plated on poly-L-Lysine (PLL)-coated coverslips. PLL coating was performed at least one day before the cell isolation. Clean coverslips were incubated in PLL hydrobromide solution MW 300,000 (Sigma, P1524) for 30 min at 37°C. Each coverslip was then removed onto a rack and flushed with Milli-Q water and aspirated 5 times. Coverslips were left to dry in a biosafety cabinet overnight.

For the isolation of cells from old animals, the concentration and incubation times for the enzymes were slightly modified to increase cell yield. The sinoatrial node explants from old animals were first incubated for 20 min in Low-Calcium Tyrode's containing twice the concentration of collagenase B used in the young (Cf = 1.08 U/ml, Roche 11088807001), followed by the same 30 min digestion with the three other enzymes at the same concentration used for young tissues. During incubation, mechanical dissociation was performed every 5-7 min. All the other steps of the protocol were the same used for young tissues.

Protein extraction and western blot

Animals were anesthetized and the heart was quickly removed and placed in ice-cold homogenization buffer. The heart was pinned down on a Sylgard®-coated 60 mm dish containing ice-cold homogenization buffer. The sinoatrial node explant was dissected and quickly transferred into a glass micro-tissue grinder (DWK, 357844) containing 100 l of lysis buffer. On ice, the tissue was grinned until totally homogenized. The sample was transferred to a 1.5 ml tube and placed in a rotator-wheel at 4°C for 2 h. Samples were centrifuged at 16,000 rfc for 20 min at 4°C. The supernatant containing solubilized proteins was transferred into a new tube and stored at -80°C. Protein concentration was determined by measuring 590 nm absorbance using Quick Start Bradford (Biorad Cat 5000205) in a Spectronic Genesis 5 plate spectrophotometer. Protein concentration obtained from a single sinoatrial node tissue ranged between 1.5 - 2.5 µg/µl. For electrophoresis, protein samples were denaturalized in SDS loading buffer for 10 min at 70°C. 25 g of protein were loaded per line on a Mini Protean TGX Precast 4-10% Biorad gel. As a reference, the ladder spectra multicolor was loaded (Thermo, 26634). Gels were run for 15 min at 50 V followed by 1 h at 130 V in TGS. Proteins were transferred onto 0.2 µm PVDF membranes (Thermo, 1704157) using an OwlTM Electroblotting system (Thermo, VEP-2) at 0.4 A and 4°C for 2 h. Membranes were stained for total protein using No-StainTM protein labeling reagent (Invitrogen, A44449), following the manufacturer's instructions. Total protein images were taken using a an iBright imaging system (Thermo). For immunoblotting, membranes were blocked in 5% Milk in TBST at RT for 1h with constant agitation. Rabbit polyclonal anti-$Ca_V1.2$ (anti-CNC1) and rabbit polyclonal anti-$Ca_V1.3$ (anti-CND1), were kindly provided by Drs. William Catterall and Ruth Westenbroek (University of Washington) and used at 1:250 dilution in blocking solution. Membranes were incubated in primary antibodies overnight at 4°C with constant agitation. The day after, membranes were washed 4x for 10 min in TBST and incubated with Goat anti-rabbit HRP-conjugated secondary antibody at 1:10,000 in blocking solution for 1h at RT with constant agitation. Membranes were washed in TBST and bands were detected using the Clarity Max Western ECL substrate (Biorad, 1705062) and the iBright imaging system. Protein abundance was calculated by measuring the area under the curve of the band intensity profile using ImageJ (NIH). Each band was normalized to total protein and reported relative to the abundance in young pacemaker samples within the same experiment.

Electrophysiology

The composition of all the solutions used for electrophysiology can be found in the Solutions section. Calcium currents were recorded using the whole-cell configuration of the patch-clamp technique in voltage-clamp mode. Isolated pacemaker cells were perfused with Tyrode's III solution at RT. Borosilicate patch pipettes with resistances of 3–6 MΩ were used. Once the gigaseal was formed, the Tyrode's III bath solution was exchanged to the I_{Ca} external solution. Current–voltage relationships were obtained by subjecting cells to a series of 20-ms depolarizing pulses from a holding potential of -75 mV to test potentials ranging from 75 to +75 mV at a 5 mV interval. The voltage dependence of channel activation (G/Gmax) was obtained from the resultant currents by converting them to conductances using the equation, $G = I_{Ca}$/(test pulse potential – reversal potential of I_{Ca}); normalized G/Gmax was plotted as a function of test potential. Currents were sampled at a frequency of 10 kHz and low-pass filtered at 2 kHz using an Axopatch 200B amplifier.

Spontaneous pacemaker action potentials were recorded in current-clamp mode using the perforated-patch configuration. Borosilicate patch pipettes with resistances of 3–6 MΩ were used. Spontaneous activity was recorded in the gap-free mode with no holding or transient current applied. Data was sampled at 10 kHz and low-pass filtered at 2 kHz using an Axopatch 200B amplifier. Action potential parameters were analyzed manually using pCLAMP 11 (Molecular Devices).

Single channel activity was recorded from cell-attached patches. Borosilicate patch pipettes with resistances of 5–7 MΩ were used. Once the giga seal was obtained, the Tyrode's III bath

solution was exchanged to single channel recording external solution. Cells were stimulated with 30 sweeps of a 200 ms square voltage pulse from a resting membrane potential of -80 mV to -30mV. Current traces were sampled at a frequency of 10 kHz and low-pass filtered at 2 kHz using an Axopatch 200B amplifier. Currents were analyzed using pCLAMP 11 (Molecular Devices). The single-channel event detection algorithm of pCLAMP was used to measure single-channel opening amplitudes and times. Recordings were filtered using a gaussian low-pass filter at 1500 KHz and the baseline was adjusted manually. Coupling coefficient was determined using a custom built macro in MATLAB

The channel coupling coefficient (κ) was calculated from single channels recording traces using a coupled Markov chain model described by Chung and Kennedy ***Chung and Kennedy*** (***1996***). The custom program was written in MATLAB and has been extensively used elsewhere ***Dixon et al.*** (***2015***); ***Moreno et al.*** (***2016***); ***Navedo et al.*** (***2010***). The activity of single channels was modeled as a first-order, discrete Markov chain, and the Markovian transition matrix was estimated from single-channel recordings and their corresponding channel opening time courses using the built-in Hidden Markov parameter estimation function in MATLAB. Elementary event amplitudes were set at 0.7 pA. The coupling coefficient (κ) is a dimensionless value ranging between 0 and 1, where 0 corresponds to fully uncoupled channels and 1 to fully coupled channels. Coupling strength was calculated as the percentage of sweeps from a cell with $\kappa > 0$.

Immucytochemistry and super-resolution microscopy

For immunostaining $Ca_V1.2$ and $Ca_V1.3$ channels in pacemaker cells, cells were isolated and plated on PLL-coated coverslips for 2 hours to attach. Gently, excess solution was removed and cells were fixed with 4% PFA in PBS for 15 min at RT. Unless stated otherwise, all the washing steps in this protocol consisted of 3 rinses with PBS followed by 3 x 5 min washes with PBS on a rocker at low speed. After washing with PFA with PBS, cells were incubated with 50 mM Glycine in PBS for 15 min at RT (aldehyde reduction), and then washed again with PBS. Cells were blocked with 3% w/v BSA - 0.25% v/v Triton X-100 in PBS (blocking solution) for 1h at RT. Primary antibodies were diluted in blocking solution to a concentration of 10 µg/mL (100 µl/coverslip) and incubated overnight at 4ºC under gentle orbital agitation. Cells were immunostained using the following antibodies: rabbit polyclonal anti-$Ca_V1.2$ (anti-CNC1), rabbit polyclonal $Ca_V1.3$ (anti-CND1), guinea pig anti-HCN4 (Alomone, AGP-004)). Anti-CNC1 and anti-CND1 were kindly provided by Drs. William Catterall and Ruth Westenbroek (University of Washington). After antibody incubation, cells were washed with PBS and incubated for 1h at RT with specific Alexa Fluor-conjugated antibodies at 2 µg/ml in blocking solution. For Airyscan imaging, Alexa Fluor 647-conjugated donkey anti-rabbit and Alexa Fluor 488-conjugated donkey anti-guinea pig were used. For super-resolution microscopy, Alexa Fluor 647-conjugated donkey anti-rabbit antibodies were used. For super-resolution microscopy, coverslips were mounted on microscope slides with a round cavity (NeoLab Migge Laborbedarf-Vertriebs GmbH, Germany) using MEA-GLOX imaging buffer and sealed with Twinsil (Picodent, Germany). The imaging buffer contained 10 mM MEA, 0.56 mg/ml glucose oxidase, 34 µg/ml catalase, and 10% w/v glucose in TN buffer (50 mM Tris-HCl pH 8, 10 mM NaCl).

A super resolution ground-state depletion system (SR-GSD, Leica) based on stochastic single-molecule localization was used to generate super-resolution images of $Ca_V1.2$ and $Ca_V1.3$ channels in pacemaker cells. The Leica SR-GSD system was equipped with 642 nm high-power lasers (2.1 kW/cm^2) and a 405 nm 30 mW laser. Images were obtained using a 160× HCX Plan-Apochromat (NA 1.43) oil-immersion lens and an EMCCD camera (iXon3 897; Andor Technology). For all experiments, the camera was running in frame-transfer mode at a frame rate of 100Hz (10 ms exposure time). Fluorescence was detected through Leica high-power TIRF 642 HP-T filter cube with an emission band-pass filter of 660–760 nm. Super-resolution localization images of $Ca_V1.2$ and $Ca_V1.3$ channel distribution were reconstructed using the coordinates of centroids obtained by

fitting single-molecule fluorescence signals with a 2D Gaussian function using LASAF software (Leica). A total of 50,000 images were used to construct the images. $Ca_V1.2$ and $Ca_V1.3$ cluster size was determined using binary masks of the images in ImageJ software (NIH).

Acknowledgments

This work was supported by grants from the US National Institutes of Health (CMM: R00 AG056595; OV: R35GM142690; LFS:R01HL144071, 5R01HL152681, 5R01HL085686), the AFAR-Glenn Foundation Junior Faculty Award (CMM), and the AFAR-Sagol Geromics Award (OV). We thank Dr. William Caterall and Dr. Ruth Westenbroek for providing the anti-L-type calcium channels antibodies used in this study. We thank Dr. Manuel Navedo for his help with the channel coupling analysis. We thank Dr. Bertil Hille and Dr. Rosie Dixon for their critical reading of the manuscript. We thank Dr. Mariya Sweetwyne for the long and fruitful sessions of scientific writing.

References

Alghamdi AM, Boyett MR, Hancox JC, Zhang H. Cardiac Pacemaker Dysfunction Arising From Different Studies of Ion Channel Remodeling in the Aging Rat Heart. Front Physiol. 2020; 11:546508. https://www.ncbi.nlm.nih.gov/pubmed/33343378, doi: 10.3389/fphys.2020.546508.

Altier C, Dubel SJ, Barrere C, Jarvis SE, Stotz SC, Spaetgens RL, Scott JD, Cornet V, De Waard M, Zamponi GW, Nargeot J, Bourinet E. Trafficking of L-type calcium channels mediated by the postsynaptic scaffolding protein AKAP79. J Biol Chem. 2002; 277(37):33598–603. https://www.ncbi.nlm.nih.gov/pubmed/12114507, doi: 10.1074/jbc.M202476200.

Amberg GC, Navedo MF, Nieves-Cintron M, Molkentin JD, Santana LF. Calcium sparklets regulate local and global calcium in murine arterial smooth muscle. J Physiol. 2007; 579(Pt 1):187–201. https://www.ncbi.nlm.nih.gov/pubmed/17158168, doi: 10.1113/jphysiol.2006.124420.

Arbel-Ganon L, Behar JA, Gomez AM, Yaniv Y. Distinct mechanisms mediate pacemaker dysfunction associated with catecholaminergic polymorphic ventricular tachycardia mutations: Insights from computational modeling. J Mol Cell Cardiol. 2020; 143:85–95. https://www.ncbi.nlm.nih.gov/pubmed/32339564, doi: 10.1016/j.yjmcc.2020.04.017.

Aziz Q, Li Y, Tinker A. Potassium channels in the sinoatrial node and their role in heart rate control. Channels (Austin). 2018; 12(1):356–366. https://www.ncbi.nlm.nih.gov/pubmed/30301404, doi: 10.1080/19336950.2018.1532255.

Baig SM, Koschak A, Lieb A, Gebhart M, Dafinger C, Nurnberg G, Ali A, Ahmad I, Sinnegger-Brauns MJ, Brandt N, Engel J, Mangoni ME, Farooq M, Khan HU, Nurnberg P, Striessnig J, Bolz HJ. Loss of Ca(v)1.3 (CACNA1D) function in a human channelopathy with bradycardia and congenital deafness. Nat Neurosci. 2011; 14(1):77–84. https://www.ncbi.nlm.nih.gov/pubmed/21131953, doi: 10.1038/nn.2694.

Baruscotti M, Bucchi A, Difrancesco D. Physiology and pharmacology of the cardiac pacemaker ("funny") current. Pharmacol Ther. 2005; 107(1):59–79. https://www.ncbi.nlm.nih.gov/pubmed/15963351, doi: 10.1016/j.pharmthera.2005.01.005.

Baudot M, Torre E, Bidaud I, Louradour J, Torrente AG, Fossier L, Talssi L, Nargeot J, Barrere-Lemaire S, Mesirca P, Mangoni ME. Concomitant genetic ablation of L-type Cav1.3 (alpha1D) and T-type Cav3.1 (alpha1G) Ca(2+) channels disrupts heart automaticity. Sci Rep. 2020; 10(1):18906. https://www.ncbi.nlm.nih.gov/pubmed/33144668, doi: 10.1038/s41598-020-76049-7.

Bechem M, Schramm M. Calcium-agonists. J Mol Cell Cardiol. 1987; 19 Suppl 2:63–75. https://www.ncbi.nlm.nih.gov/pubmed/2442401, doi: 10.1016/s0022-2828(87)80005-6.

Birnie D, Williams K, Guo A, Mielniczuk L, Davis D, Lemery R, Green M, Gollob M, Tang A. Reasons for escalating pacemaker implants. Am J Cardiol. 2006; 98(1):93–7. https://www.ncbi.nlm.nih.gov/pubmed/16784928, doi: 10.1016/j.amjcard.2006.01.069.

Brown AM, Kunze DL, Yatani A. The agonist effect of dihydropyridines on Ca channels. Nature. 1984; 311(5986):570–2. https://www.ncbi.nlm.nih.gov/pubmed/6207438, doi: 10.1038/311570a0.

Choi S, Vivas O, Baudot M, Moreno CM. Aging Alters the Formation and Functionality of Signaling Microdomains Between L-type Calcium Channels and beta2-Adrenergic Receptors in Cardiac Pacemaker Cells. Front Physiol. 2022; 13:805909. https://www.ncbi.nlm.nih.gov/pubmed/35514336, doi: 10.3389/fphys.2022.805909.

Chung SH, Kennedy RA. Coupled Markov chain model: characterization of membrane channel currents with multiple conductance sublevels as partially coupled elementary pores. Math Biosci. 1996; 133(2):111–37. https://www.ncbi.nlm.nih.gov/pubmed/8718705, doi: 10.1016/0025-5564(95)00084-4.

Davare MA, Dong F, Rubin CS, Hell JW. The A-kinase anchor protein MAP2B and cAMP-dependent protein kinase are associated with class C L-type calcium channels in neurons. J Biol Chem. 1999; 274(42):30280–7. https://www.ncbi.nlm.nih.gov/pubmed/10514522, doi: 10.1074/jbc.274.42.30280.

Del Villar SG, Voelker TL, Westhoff M, Reddy GR, Spooner HC, Navedo MF, Dickson EJ, Dixon RE. beta-Adrenergic control of sarcolemmal CaV1.2 abundance by small GTPase Rab proteins. Proc Natl Acad Sci U S A. 2021; 118(7). https://www.ncbi.nlm.nih.gov/pubmed/33558236, doi: 10.1073/pnas.2017937118.

DiFrancesco D. The pacemaker current (I(f)) plays an important role in regulating SA node pacemaker activity. Cardiovasc Res. 1995; 30(2):307–8. https://www.ncbi.nlm.nih.gov/pubmed/7585819.

Dixon RE, Moreno CM, Yuan C, Opitz-Araya X, Binder MD, Navedo MF, Santana LF. Graded Ca(2)(+)/calmodulin-dependent coupling of voltage-gated CaV1.2 channels. Elife. 2015; 4. https://www.ncbi.nlm.nih.gov/pubmed/25714924, doi: 10.7554/eLife.05608.

Dolphin AC. Calcium channel auxiliary alpha2delta and beta subunits: trafficking and one step beyond. Nat Rev Neurosci. 2012; 13(8):542–55. https://www.ncbi.nlm.nih.gov/pubmed/22805911, doi: 10.1038/nrn3311.

Fenske S, Probstle R, Auer F, Hassan S, Marks V, Pauza DH, Biel M, Wahl-Schott C. Comprehensive multilevel in vivo and in vitro analysis of heart rate fluctuations in mice by ECG telemetry and electrophysiology. Nat Protoc. 2016; 11(1):61–86. https://www.ncbi.nlm.nih.gov/pubmed/26658468, doi: 10.1038/nprot.2015.139.

Finlin BS, Crump SM, Satin J, Andres DA. Regulation of voltage-gated calcium channel activity by the Rem and Rad GTPases. Proc Natl Acad Sci U S A. 2003; 100(24):14469–74. https://www.ncbi.nlm.nih.gov/pubmed/14623965, doi: 10.1073/pnas.2437756100.

Flurkey K, Currer JM, Harrison DE. In: Fox JG DMNCQFSA Barthold SW, editor. Mouse models in aging research, vol. 3, 2nd ed. Elsevier; 2007. p. 637–72.

Gao T, Yatani A, Dell'Acqua ML, Sako H, Green SA, Dascal N, Scott JD, Hosey MM. cAMP-dependent regulation of cardiac L-type Ca2+ channels requires membrane targeting of PKA and phosphorylation of channel subunits. Neuron. 1997; 19(1):185–96. https://www.ncbi.nlm.nih.gov/pubmed/9247274, doi: 10.1016/s0896-6273(00)80358-x.

Ghosh D, Nieves-Cintron M, Tajada S, Brust-Mascher I, Horne MC, Hell JW, Dixon RE, Santana LF, Navedo MF. Dynamic L-type CaV1.2 channel trafficking facilitates CaV1.2 clustering and cooperative gating. Biochim Biophys Acta Mol Cell Res. 2018; 1865(9):1341–1355. https://www.ncbi.nlm.nih.gov/pubmed/29959960, doi: 10.1016/j.bbamcr.2018.06.013.

Hatch FS. Age-associated changes to calcium handling proteins across the whole heart. Ph.D. thesis. Thesis; 2012.

Hess P, Lansman JB, Tsien RW. Different modes of Ca channel gating behaviour favoured by dihydropyridine Ca agonists and antagonists. Nature. 1984; 311(5986):538–44. https://www.ncbi.nlm.nih.gov/pubmed/6207437, doi: 10.1038/311538a0.

Hille B. Ion channels of excitable membranes. Third ed.; 2001.

Hong TT, Smyth JW, Chu KY, Vogan JM, Fong TS, Jensen BC, Fang K, Halushka MK, Russell SD, Colecraft H, Hoopes CW, Ocorr K, Chi NC, Shaw RM. BIN1 is reduced and Cav1.2 trafficking is impaired in human failing cardiomyocytes. Heart Rhythm. 2012; 9(5):812–20. https://www.ncbi.nlm.nih.gov/pubmed/22138472, doi: 10.1016/j.hrthm.2011.11.055.

Hong TT, Smyth JW, Gao D, Chu KY, Vogan JM, Fong TS, Jensen BC, Colecraft HM, Shaw RM. BIN1 localizes the L-type calcium channel to cardiac T-tubules. PLoS Biol. 2010; 8(2):e1000312. https://www.ncbi.nlm.nih.gov/pubmed/20169111, doi: 10.1371/journal.pbio.1000312.

Huang X, Du Y, Yang P, Lin S, Xi Y, Yang Z, Ma A. Age-dependent alterations of voltage-gated Na(+) channel isoforms in rat sinoatrial node. Mech Ageing Dev. 2015; 152:80–90. https://www.ncbi.nlm.nih.gov/pubmed/26528804, doi: 10.1016/j.mad.2015.10.003.

Huang X, Yang P, Yang Z, Zhang H, Ma A. Age-associated expression of HCN channel isoforms in rat sinoatrial node. Exp Biol Med (Maywood). 2016; 241(3):331–9. https://www.ncbi.nlm.nih.gov/pubmed/26341471, doi: 10.1177/1535370215603515.

Jensen PN, Gronroos NN, Chen LY, Folsom AR, deFilippi C, Heckbert SR, Alonso A. Incidence of and risk factors for sick sinus syndrome in the general population. J Am Coll Cardiol. 2014; 64(6):531–8. https://www.ncbi.nlm.nih.gov/pubmed/25104519, doi: 10.1016/j.jacc.2014.03.056.

Jones SA, Boyett MR, Lancaster MK. Declining into failure: the age-dependent loss of the L-type calcium channel within the sinoatrial node. Circulation. 2007; 115(10):1183–90. https://www.ncbi.nlm.nih.gov/pubmed/17339548, doi: 10.1161/CIRCULATIONAHA.106.663070.

Kokubun S, Reuter H. Dihydropyridine derivatives prolong the open state of Ca channels in cultured cardiac cells. Proc Natl Acad Sci U S A. 1984; 81(15):4824–7. https://www.ncbi.nlm.nih.gov/pubmed/6205402, doi: 10.1073/pnas.81.15.4824.

Larson ED, St Clair JR, Sumner WA, Bannister RA, Proenza C. Depressed pacemaker activity of sinoatrial node myocytes contributes to the age-dependent decline in maximum heart rate. Proc Natl Acad Sci U S A. 2013; 110(44):18011–6. https://www.ncbi.nlm.nih.gov/pubmed/24128759, doi: 10.1073/pnas.1308477110.

Liu G, Papa A, Katchman AN, Zakharov SI, Roybal D, Hennessey JA, Kushner J, Yang L, Chen BX, Kushnir A, Dangas K, Gygi SP, Pitt GS, Colecraft HM, Ben-Johny M, Kalocsay M, Marx SO. Mechanism of adrenergic CaV1.2 stimulation revealed by proximity proteomics. Nature. 2020; 577(7792):695–700. https://www.ncbi.nlm.nih.gov/pubmed/31969708, doi: 10.1038/s41586-020-1947-z.

Magyar J, Kiper CE, Sievert G, Cai W, Shi GX, Crump SM, Li L, Niederer S, Smith N, Andres DA, Satin J. Rem-GTPase regulates cardiac myocyte L-type calcium current. Channels (Austin). 2012; 6(3):166–73. https://www.ncbi.nlm.nih.gov/pubmed/22854599, doi: 10.4161/chan.20192.

Mangoni ME, Couette B, Bourinet E, Platzer J, Reimer D, Striessnig J, Nargeot J. Functional role of L-type Cav1.3 Ca2+ channels in cardiac pacemaker activity. Proc Natl Acad Sci U S A. 2003; 100(9):5543–8. https://www.ncbi.nlm.nih.gov/pubmed/12700358, doi: 10.1073/pnas.0935295100.

Mangoni ME, Nargeot J. Genesis and regulation of the heart automaticity. Physiol Rev. 2008; 88(3):919–82. https://www.ncbi.nlm.nih.gov/pubmed/18626064, doi: 10.1152/physrev.00018.2007.

Marcus B, Gillette PC, Garson J A. Intrinsic heart rate in children and young adults: an index of sinus node function isolated from autonomic control. Am Heart J. 1990; 119(4):911–6. https://www.ncbi.nlm.nih.gov/pubmed/2321510, doi: 10.1016/s0002-8703(05)80331-x.

Marshall MR, Clark r J P, Westenbroek R, Yu FH, Scheuer T, Catterall WA. Functional roles of a C-terminal signaling complex of CaV1 channels and A-kinase anchoring protein 15 in brain neurons. J Biol Chem. 2011; 286(14):12627–39. https://www.ncbi.nlm.nih.gov/pubmed/21224388, doi: 10.1074/jbc.M110.175257.

Mesirca P, Torrente AG, Mangoni ME. Functional role of voltage gated Ca(2+) channels in heart automaticity. Front Physiol. 2015; 6:19. https://www.ncbi.nlm.nih.gov/pubmed/25698974, doi: 10.3389/fphys.2015.00019.

Milanesi R, Bucchi A, Baruscotti M. The genetic basis for inherited forms of sinoatrial dysfunction and atrioventricular node dysfunction. J Interv Card Electrophysiol. 2015; 43(2):121–34. https://www.ncbi.nlm.nih.gov/pubmed/25863800, doi: 10.1007/s10840-015-9998-z.

Moreno CM, Dixon RE, Tajada S, Yuan C, Opitz-Araya X, Binder MD, Santana LF. Ca(2+) entry into neurons is facilitated by cooperative gating of clustered CaV1.3 channels. Elife. 2016; 5. https://www.ncbi.nlm.nih.gov/pubmed/27187148, doi: 10.7554/eLife.15744.

Navedo MF, Cheng EP, Yuan C, Votaw S, Molkentin JD, Scott JD, Santana LF. Increased coupled gating of L-type Ca2+ channels during hypertension and Timothy syndrome. Circ Res. 2010; 106(4):748–56. https://www.ncbi.nlm.nih.gov/pubmed/20110531, doi: 10.1161/CIRCRESAHA.109.213363.

Nystoriak MA, Nieves-Cintron M, Patriarchi T, Buonarati OR, Prada MP, Morotti S, Grandi E, Fernandes JD, Forbush K, Hofmann F, Sasse KC, Scott JD, Ward SM, Hell JW, Navedo MF. Ser1928 phosphorylation by PKA stimulates the L-type Ca2+ channel CaV1.2 and vasoconstriction during acute hyperglycemia and diabetes. Sci Signal. 2017; 10(463). https://www.ncbi.nlm.nih.gov/pubmed/28119464, doi: 10.1126/scisignal.aaf9647.

Olson PA, Tkatch T, Hernandez-Lopez S, Ulrich S, Ilijic E, Mugnaini E, Zhang H, Bezprozvanny I, Surmeier DJ. G-protein-coupled receptor modulation of striatal CaV1.3 L-type Ca2+ channels is dependent on a Shank-binding domain. J Neurosci. 2005; 25(5):1050–62. https://www.ncbi.nlm.nih.gov/pubmed/15689540, doi: 10.1523/JNEUROSCI.3327-04.2005.

Ostchega Y, Porter KS, Hughes J, Dillon CF, Nwankwo T. Resting pulse rate reference data for children, adolescents, and adults: United States, 1999-2008. Natl Health Stat Report. 2011; (41):1–16. https://www.ncbi.nlm.nih.gov/pubmed/21905522.

Papa A, Kushner J, Hennessey JA, Katchman AN, Zakharov SI, Chen BX, Yang L, Lu R, Leong S, Diaz J, Liu G, Roybal D, Liao X, Del Rivero Morfin PJ, Colecraft HM, Pitt GS, Clarke O, Topkara V, Ben-Johny M, Marx SO. Adrenergic CaV1.2 Activation via Rad Phosphorylation Converges at alpha1C I-II Loop. Circ Res. 2021; 128(1):76–88. https://www.ncbi.nlm.nih.gov/pubmed/33086983, doi: 10.1161/CIRCRESAHA.120.317839.

Peters CH, Sharpe EJ, Proenza C. Cardiac Pacemaker Activity and Aging. Annu Rev Physiol. 2020; 82:21–43. https://www.ncbi.nlm.nih.gov/pubmed/31756134, doi: 10.1146/annurev-physiol-021119-034453.

Platzer J, Engel J, Schrott-Fischer A, Stephan K, Bova S, Chen H, Zheng H, Striessnig J. Congenital deafness and sinoatrial node dysfunction in mice lacking class D L-type Ca2+ channels. Cell. 2000; 102(1):89–97. https://www.ncbi.nlm.nih.gov/pubmed/10929716, doi: 10.1016/s0092-8674(00)00013-1.

Pym E, Sasidharan N, Thompson-Peer KL, Simon DJ, Anselmo A, Sadreyev R, Hall Q, Nurrish S, Kaplan JM. Shank is a dose-dependent regulator of Cav1 calcium current and CREB target expression. Elife. 2017; 6. https://www.ncbi.nlm.nih.gov/pubmed/28477407, doi: 10.7554/eLife.18931.

Robinson S, Dill DB, Tzankoff SP, Wagner JA, Robinson RD. Longitudinal studies of aging in 37 men. J Appl Physiol. 1975; 38(2):263–7. https://www.ncbi.nlm.nih.gov/pubmed/1120749, doi: 10.1152/jappl.1975.38.2.263.

Sharpe EJ, Larson ED, Proenza C. Cyclic AMP reverses the effects of aging on pacemaker activity and If in sinoatrial node myocytes. J Gen Physiol. 2017; 149(2):237–247. https://www.ncbi.nlm.nih.gov/pubmed/28057842, doi: 10.1085/jgp.201611674.

Tanaka H, Monahan KD, Seals DR. Age-predicted maximal heart rate revisited. J Am Coll Cardiol. 2001; 37(1):153–6. https://www.ncbi.nlm.nih.gov/pubmed/11153730, doi: 10.1016/s0735-1097(00)01054-8.

Tellez JO, McZewski M, Yanni J, Sutyagin P, Mackiewicz U, Atkinson A, Inada S, Beresewicz A, Billeter R, Dobrzynski H, Boyett MR. Ageing-dependent remodelling of ion channel and Ca2+ clock genes underlying sino-atrial node pacemaking. Exp Physiol. 2011; 96(11):1163–78. https://www.ncbi.nlm.nih.gov/pubmed/21724736, doi: 10.1113/expphysiol.2011.057752.

Thomas G, Chung M, Cohen CJ. A dihydropyridine (Bay k 8644) that enhances calcium currents in guinea pig and calf myocardial cells. A new type of positive inotropic agent. Circ Res. 1985; 56(1):87–96. https://www.ncbi.nlm.nih.gov/pubmed/2578336, doi: 10.1161/01.res.56.1.87.

Torrente AG, Mesirca P, Neco P, Rizzetto R, Dubel S, Barrere C, Sinegger-Brauns M, Striessnig J, Richard S, Nargeot J, Gomez AM, Mangoni ME. L-type Cav1.3 channels regulate ryanodine receptor-dependent Ca2+ release during sino-atrial node pacemaker activity. Cardiovasc Res. 2016; 109(3):451–61. https://www.ncbi.nlm.nih.gov/pubmed/26786159, doi: 10.1093/cvr/cvw006.

Wang YY, Mesirca P, Marques-Sule E, Zahradnikova J A, Villejoubert O, D'Ocon P, Ruiz C, Domingo D, Zorio E, Mangoni ME, Benitah JP, Gomez AM. RyR2R420Q catecholaminergic polymorphic ventricular tachycardia mutation induces bradycardia by disturbing the coupled clock pacemaker mechanism. JCI Insight. 2017; 2(8). https://www.ncbi.nlm.nih.gov/pubmed/28422759, doi: 10.1172/jci.insight.91872.

Xu X, Marx SO, Colecraft HM. Molecular mechanisms, and selective pharmacological rescue, of Rem-inhibited CaV1.2 channels in heart. Circ Res. 2010; 107(5):620–30. https://www.ncbi.nlm.nih.gov/pubmed/20616312, doi: 10.1161/CIRCRESAHA.110.224717.

Zhang H, Maximov A, Fu Y, Xu F, Tang TS, Tkatch T, Surmeier DJ, Bezprozvanny I. Association of CaV1.3 L-type calcium channels with Shank. J Neurosci. 2005; 25(5):1037–49. https://www.ncbi.nlm.nih.gov/pubmed/15689539, doi: 10.1523/JNEUROSCI.4554-04.2005.

Zhao Y, Huang G, Wu J, Wu Q, Gao S, Yan Z, Lei J, Yan N. Molecular Basis for Ligand Modulation of a Mammalian Voltage-Gated Ca(2+) Channel. Cell. 2019; 177(6):1495–1506 e12. https://www.ncbi.nlm.nih.gov/pubmed/31150622, doi: 10.1016/j.cell.2019.04.043.